Elevated-temperature cyclic deformation mechanisms of CoCrNi in comparison to CoCrFeMnNi

Kaiju Lu[1*], Fabian Knöpfle[1], Ankur Chauhan[1,2], Dimitri Litvinov[1], Mike Schneider[3], Guillaume Laplanche[3], and Jarir Aktaa[1]

[1]Institute for Applied Materials, Karlsruhe Institute of Technology (KIT), Hermann-von-Helmholtz-Platz 1, 76344 Eggenstein-Leopoldshafen, Germany

[2]Department of Materials Engineering, Indian Institute of Science, Bengaluru, 560012, Karnataka, India

[3]Institut für Werkstoffe, Ruhr-Universität Bochum, D-44801, Bochum, Germany

Email: *kaiju.lu@kit.edu; kaiju.lu@hotmail.com

Abstract

We report the cyclic deformation behavior of CoCrNi at 550 °C under a strain amplitude of ± 0.5% and compare it to that of CoCrFeMnNi. CoCrNi manifests cyclic hardening followed by minor softening and a near-steady state until failure. Transmission electron microscopy investigations of CoCrNi revealed that increasing the number of cycles from 10 to 2500/5000 leads to a transition of dislocation arrangements from slip bands to tangles. Compared to CoCrFeMnNi, CoCrNi exhibits higher strength, longer lifetime and persistent serrated flow. Owing to its lower stacking fault energy (even at 550 °C), planar slip is more pronounced in CoCrNi than CoCrFeMnNi, which additionally shows wavy slip.

Keywords: Multi-principal element alloy; Fatigue; Transmission electron microscopy; Dislocation; Elevated-temperature.

Over the past two decades, multi-principal element alloys (MPEAs) have been attracting increasing interest [1-3]. The most explored single-phase and face-centered cubic (FCC) MPEAs are the equiatomic CoCrNi and CoCrFeMnNi alloys. These two alloys are regarded as model MPEAs and promising candidates for next-generation engineering applications due to their excellent combination of mechanical properties [1-5]. At elevated temperatures, despite their superior oxidation and corrosion resistance [6], the inadequate strength of CoCrNi-based FCC MPEAs limits their direct applications [7]. However, the advancement of oxide dispersion-strengthened MPEAs and high-entropy superalloys with a CoCrNi matrix has increased their strength to a level comparable or even superior to Inconel and Ni-based superalloys [7]. Therefore, there is an urgent need to understand the deformation mechanisms of the CoCrNi matrix at elevated temperatures, as it is the prerequisite for constructing physics-based models for more complex CoCrNi-based MPEAs [7].

Recently, much attention has been placed on the high-temperature performance of MPEAs, such as tension/compression [8-10], tensile creep [7, 11-13] and low-cycle fatigue (LCF) [14, 15] properties. Despite many endeavors having unveiled their LCF behavior at room temperature (RT) [14-21], limited attention has been paid to their LCF response at elevated temperatures (only for CoCrFeMnNi) [14, 15]. For instance, CoCrFeMnNi has been reported to exhibit fatigue resistance comparable to (or even better than) conventional steels at 550 °C (which lies within the proposed operating temperature range of advanced power plants and nuclear reactors [22-24]) [14].

Furthermore, compared to CoCrFeMnNi, CoCrNi exhibits even superior LCF life at RT. This was mainly attributed to its more pronounced planar slip (along with occasional cross slip) and lower stacking fault energy (SFE, of 22 ± 4 mJ/m^2 [4]) [16] than that of CoCrFeMnNi (*i.e.*, prevalent cross slip [17] and SFE of 30 ± 5 mJ/m^2 [25, 26]) at RT. However, CoCrNi's LCF response at elevated temperatures (*e.g.*, 550 °C) remains unexplored. At high temperatures, it is well-known that dynamic recovery processes such as cross-slip are promoted [27, 28], and the SFE of an FCC material increases with increasing temperature [29, 30], suggesting that cyclic deformation mechanisms should

be strongly temperature-dependent [15]. Consequently, this work aims to fill this gap and provide underlying deformation mechanisms at 550 °C (emphasizing the defects involved).

Cylindrical specimens (gauge diameter: 2 mm and length: 7.6 mm) were machined out from the batches of equiatomic CoCrNi used in [16], where the processing details can be found. Before testing, the specimens were annealed at 825 °C for 1 h, resulting in a fully recrystallized and single-phase FCC microstructure with equiaxed grains (average grain size of ~ 7 µm) and a low initial dislocation density (see Fig. A1).

The strain-controlled LCF-tests were carried out at 550 °C in the air under a typical strain amplitude of ± 0.5%, following the procedure used in our previous study [14]. The strain amplitude of 0.5% is chosen to ensure the lifetime is within the LCF regime. Fatigue tests were either performed until rupture or interrupted (after 10 and 2500 cycles) to investigate the microstructural evolution. For this purpose, conventional bright-field (BF) and weak-beam dark-field (WBDF) imaging were obtained using an FEI Tecnai F20 transmission electron microscope (TEM) operating at 200 kV. High-angle annular dark-field (HAADF) scanning TEM (STEM), energy-dispersive X-ray spectroscopy (EDS) and selected area electron diffraction (SAED) analyses were carried out using a Talos F200X TEM (Thermo Scientific) with a Super X-EDS system. TEM samples were prepared by mechanical grinding, polishing and twin-jet electro-polishing, see Ref. [17]. Fracture surface investigations were carried out by employing a Zeiss EVO MA 10 SEM equipped with a Bruker EDS detector.

The tensile peak stress *versus* the number of cycles curve and the hysteresis loops for two typical cycles (*e.g.*, 2nd and half-life cycles) of CoCrNi are presented in Fig. 1a and 1b, respectively. For comparison, the results from Ref. [14] obtained for CoCrFeMnNi with similar grain size and tested under the same condition are also plotted in Fig. 1.

Similar to that of CoCrFeMnNi, the cyclic stress response of CoCrNi exhibits an initial cyclic hardening (increase in peak stress), followed by minor softening and a near-steady state (with minor changes in peak stress, covering the majority of the lifetime)

until failure (see orange curve in Fig. 1a). Noticeably, CoCrNi shows higher cyclic stress and a longer lifetime than CoCrFeMnNi. CoCrNi's higher cyclic stress is related to its higher solid solution hardening and grain boundary strengthening [31]. The reason for its longer life will be discussed later in light of our microstructural investigations.
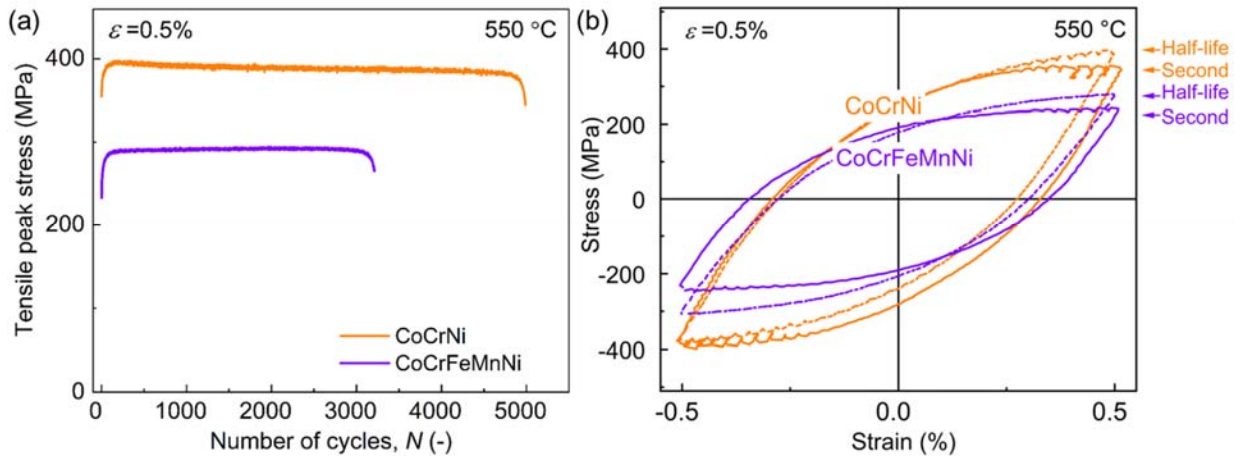
Fig. 1. (a) Evolution of tensile peak stress per cycle, (b) second and half-life stress-strain hysteresis loops for CoCrNi tested at 550 °C under a strain amplitude of 0.5%. For comparison, the results of CoCrFeMnNi tested under the same condition are also provided, see Ref. [14].

The hysteresis loops of CoCrNi at two typical cycles (*e.g.*, 2 and 2500) display serrated plastic flow, see Fig. 1b. This is in contrast to the behavior of CoCrFeMnNi, where the serrated flow was observed during the first ten cycles and disappeared afterwards [14]. In addition, the inelastic strain experienced per cycle (*i.e.*, the half-width of a hysteresis loop) is ~5% lower in CoCrNi than CoCrFeMnNi (Fig. 1b).

To probe the underlying reasons for the superior resistance of CoCrNi to LCF at 550 °C, TEM micrographs of specimens tested up to 10, 2500 (half-life), and ~ 5000 (end-life) are shown in Fig. 2 and Fig. 3, respectively. After 10 cycles (hardening stage), the dislocation density strongly increased compared to the recrystallized state (compare Fig. 2 and Fig. A1) and dislocations are organized in the form of planar slip bands, see Fig. 2a-b. These slip bands are found to consist of partial dislocations bounded by stacking

fault ribbons (SFs); see WBDF micrograph in Fig. 2b. These observations demonstrate the planar slip of dislocations during the hardening stage.
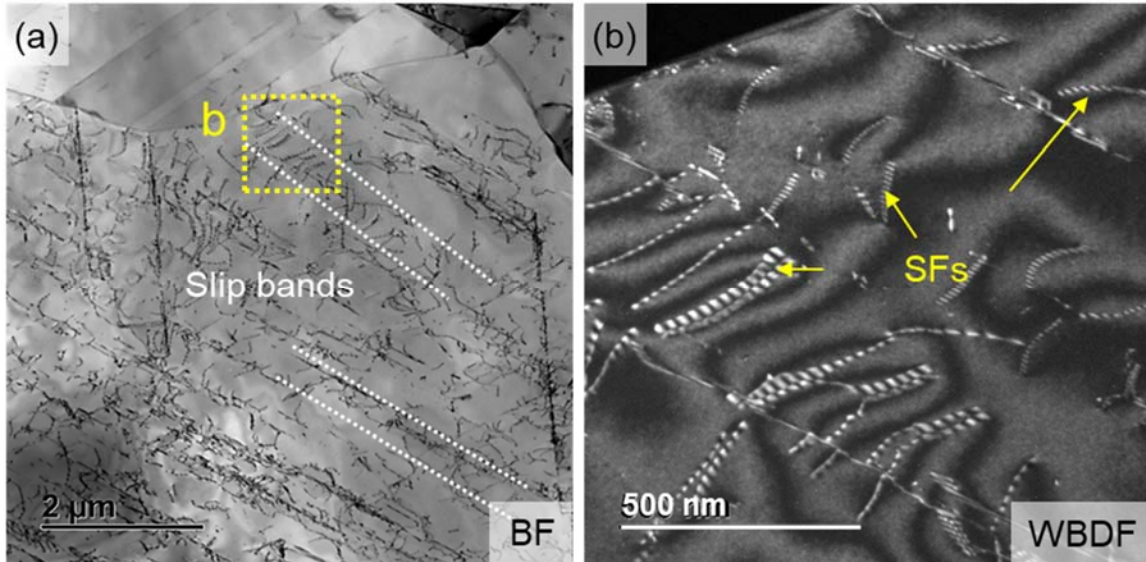
Fig. 2. TEM micrographs of the CoCrNi alloy tested at 550 °C under a strain amplitude of 0.5% up to 10 cycles. (a) BF and (b) WBDF micrographs.

After 2500 cycles and ~5000 cycles (both within the near-steady-state regime), the deformed microstructure showcases dislocation tangles homogeneously distributed in most grains (Fig. 3). These tangles are also composed of Shockley partial pairs with an SF in between (see Fig. 3b and d). Notably, no deformation twins or hexagonal close-packed martensite variants were observed under the investigated LCF conditions. This is probably due to the low applied strain/stress levels and the fact that our alloy has a fine grain size of ~7 μm, *i.e.*, a reduction of grain size is known to decrease the tendency for deformation twinning and martensitic transformation.
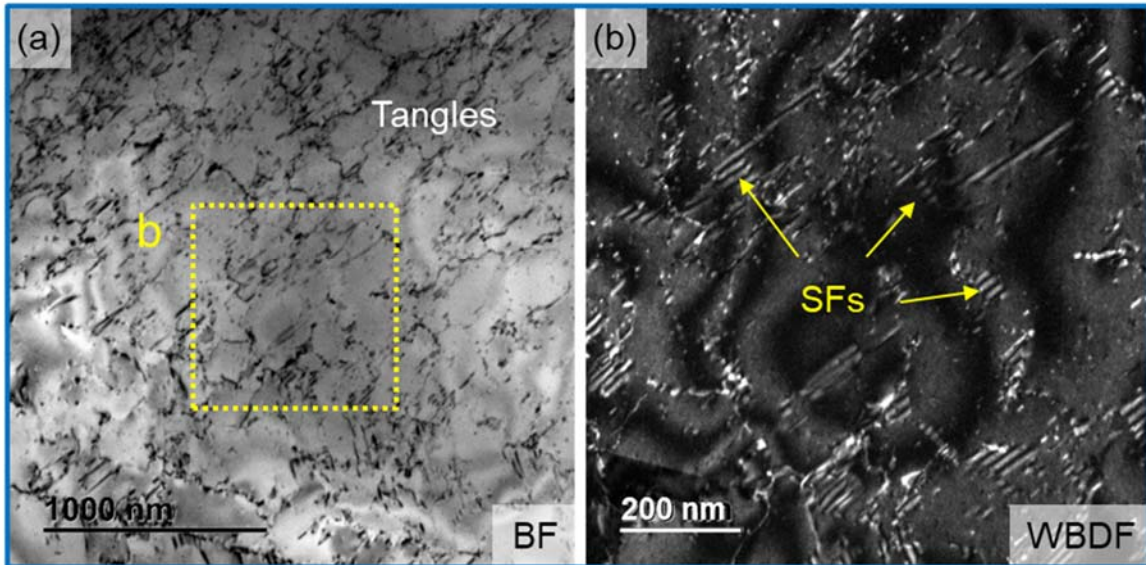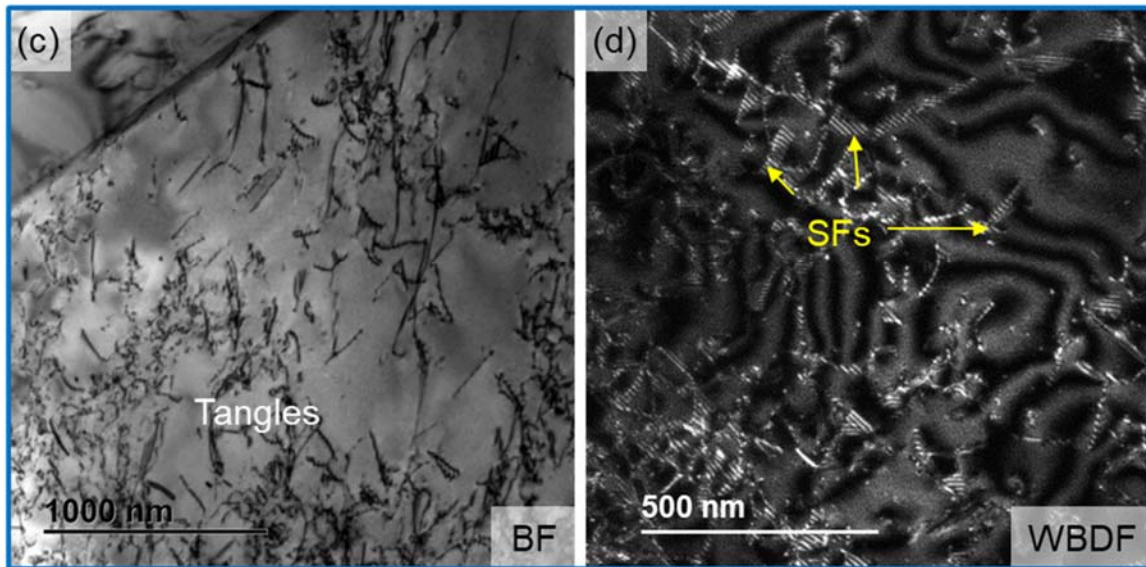
Fig. 3. Microstructural evolution in CoCrNi during LCF-testing at 550 °C under a strain amplitude of 0.5%. (a, c) BF and (b, d) WBDF micrographs. (a-b) Dislocation microstructures at the half-life (2500 cycles) and (c-d) end-life (~5000 cycles).

Additionally, STEM-EDS investigations revealed the heterogeneous precipitation of a secondary phase (see areas 1 and 2 in Fig. 4) at grain boundaries in post-fractured

CoCrNi. EDS mapping along with SAED patterns (Fig. 4) showed that these precipitates are Cr-rich (~64–73 at.% Cr) $M_{23}C_6$ carbides with an FCC structure and a lattice parameter of ~10.64 Å. Nevertheless, it is worth mentioning that the volume fraction of these carbides is extremely small (~0.003), and it is unlikely that these carbides affect the fatigue resistance of CoCrNi at 550 °C.
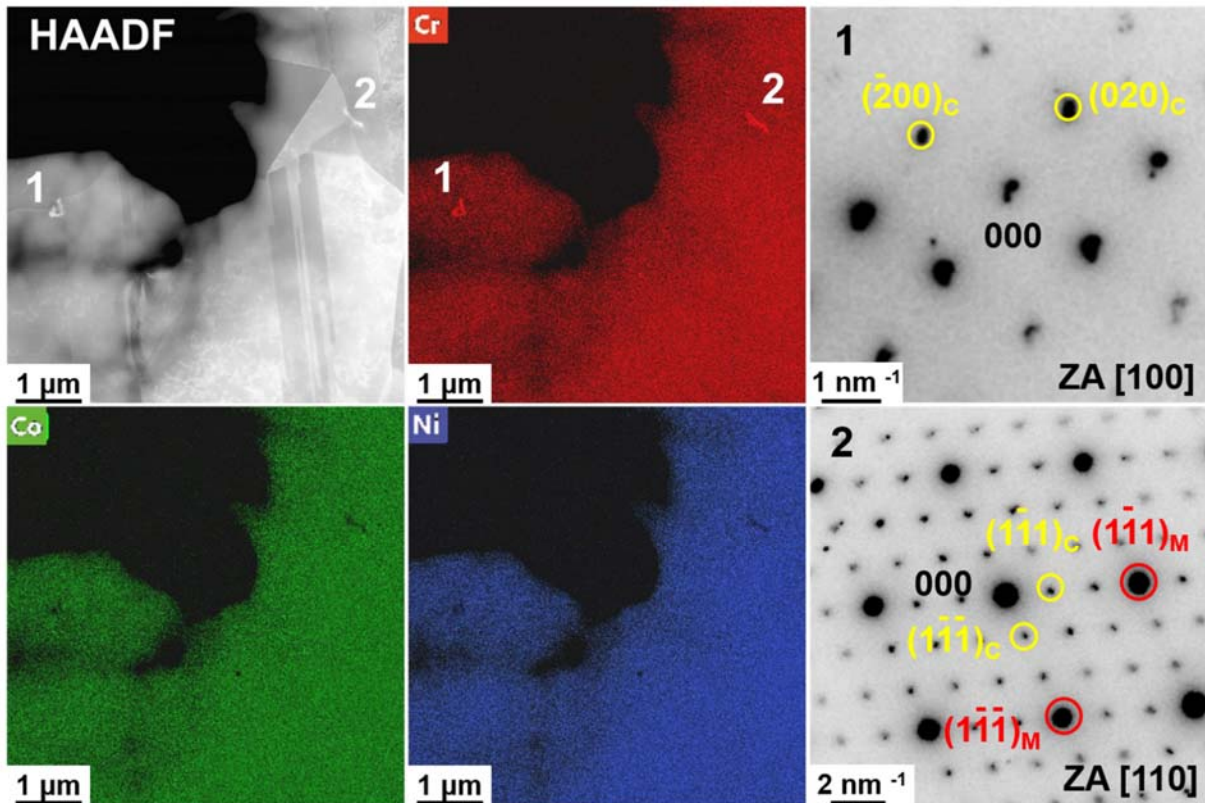
Fig. 4. HAADF micrograph and EDS elemental maps showing Cr-rich secondary phases indicated by numbers 1 and 2 from post-fractured (*i.e.*, end-life) CoCrNi tested at 550 °C under a strain amplitude of 0.5%. The precipitates are Cr-rich $M_{23}C_6$ carbides, as shown by the SAED patterns taken along the [100] and [110] zone axes where the subscripts "C" and "M" refers to carbides and matrix, respectively.

Current TEM investigations for post-fatigued CoCrNi revealed its cyclic deformation mechanisms at 550 °C. Specifically, although dislocation structures changed from planar slip bands to tangles with increasing cycle number, the planar slip of dislocations prevailed at 550 °C. Compared to the previously reported deformation mode at RT (*i.e.*,

prevalent planar slip bands and occasional wavy substructures) [16], no wavy/cross-slip induced dislocation substructures (including persistent slip bands (PSBs), walls, and cells) were observed at 550 °C. This observation is inconsistent with the hypothesis that cross-slip in FCC crystals, as a thermally activated event, is assumed to be enhanced at elevated temperatures [29, 30].

However, the pronounced planar slip and no evidence of wavy walls/cells at 550 °C can be explained as follows. *Firstly,* the prevailing planar slip can be attributed to the material's low SFE even at 550 °C, as a low SFE promotes the dissociation of perfect dislocations into Shockley partials. The SFE of CoCrNi at RT has been experimentally determined to be 22 ± 4 mJ/m^2 [4]. Although the SFE value in FCC alloys increases with temperature [27, 28], this work suggests that, with increasing temperature from RT to 550 °C, the SFE of FCC CoCrNi did not change significantly (*i.e.*, introduced a noticeable change in slip mode). This is in line with the observations reported for a Co-30wt.%Cr-15wt.%Ni alloy, whose SFE remained low (*i.e.*, from ~ 15 mJ/m^2 to ~ 22 mJ/m^2) with increasing temperature from RT to 800 K [27]. *Secondly*, since cross slip is influenced by both stress/strain level [17] and thermal activation [29], the applied strain amplitude (0.5%) and/or temperature herein (*i.e.*, 550 °C, which is close to 0.5 T_s, where T_s is the solidus temperature of the CoCrNi alloy) may not be high enough to activate extensive cross slip. Similarly, upon cycling conventional austenitic steels with a low SFE (*e.g.*, 316L-type steel), the cross slip does not play a vital role at temperatures below 600 °C (*e.g.*, planar slip bands dominated at 550 °C) [32, 33]. *Thirdly*, at elevated temperatures, Suzuki segregation (*i.e.*, segregation of solutes into SFs) may increase the SF width and thus hinder cross slip [15]. The presence of Suzuki segregation at SFs needs further dedicated investigations.

The observed evolution of dislocation structures from slip bands to tangles can be associated with the cyclic stress response of CoCrNi at 550 °C (Fig. 1a). Specifically, the initial cyclic hardening is related to an increase in dislocation density and the formation of pile-ups against grain boundaries (see Fig. 2), which contribute to increased intergranular back stresses [34]. Thereafter, with increasing cycle number (accompanied

by an increase in applied stress), dislocations from different slip systems are activated, and their interactions yield to the formation of tangles (Fig. 3). Upon further cycling, both dislocation density and their configuration attain quasi-equilibrium state, leading to a near-steady state of peak stresses.

Comparing the cyclic stress response of CoCrNi at 550 °C and RT, the temperature-dependent deformation behavior can be noticed. The main difference lies in the extent of cyclic softening, which is prominent at RT [16], but less pronounced at 550 °C (*e.g.*, see Fig. A3). The latter could be ascribed to the absence of wavy dislocation walls/cells (and in-between channels) at 550 °C. Specifically, since the dislocation-free channels (between the walls/cells) were not extensively formed at 550 °C, dislocations did not have enough free path for their easy motion [17], giving rise to less pronounced softening. However, as compared to the CoCrFeMnNi at 550 °C (where dislocations density and their configuration reached a quasi-equilibrium state [14]), the minor softening in CoCrNi at 550 °C can be attributed to the reduction of the dislocation density in the slip bands, which contributes to lower intergranular back stresses [34, 35].

The dominant planar slip activity can be further linked to the observed serrated flow at 550 °C (Fig. 1b). The serrated flow in FCC steels and CoCrFeMnNi at elevated temperatures has been usually attributed to dynamic strain aging, *i.e.*, a continuous process of Shockley partials bounded by a SF being pinned and unpinned by solute atoms [9, 14, 36-38]. Likewise, in the CoCrNi MPEA, partial dislocations bounded by SFs, moving in a planar manner upon cycling at 550 °C, can be effectively pinned and unpinned by one of the solutes (either Co, Cr, or Ni) or more. As serrated flow appeared in CoCrNi but not in the equiatomic CoNi alloy upon tensile straining at 400 °C [39], it is suggested that the Cr diffusion play an important role for the serrated flow in CoCrNi. This may be related to the fact that Cr diffuses at a much faster rate than Co and Ni in CrFeCoNi alloys [40]. Additionally, while the serrated flow in CoCrFeMnNi gradually disappears, it persists in CoCrNi (Fig. 1b). This is related to the prevalence of planar slip in CoCrNi throughout the LCF testing duration, which is different from the onset of wavy slip in CoCrFeMnNi (*i.e.*, the formation of dislocation walls/cells due to its higher SFE

(compared to CoCrNi), where dislocations may glide smoothly over shorter distances as a result of the relatively favorable cross-slip condition) [15].

A comparison of the lifetimes of CoCrFeMnNi and CoCrNi suggests that the predominant planar slip in CoCrNi is also responsible for its longer fatigue life (Fig. 1a). This is because the planar slip in CoCrNi is relatively "more reversible" [41] than the wavy slip in CoCrFeMnNi, resulting in a longer lifetime in the former case. Besides, planar slip ensures more homogeneous deformation, suppressing the formation of localized dislocation substructures (*e.g.*, PSBs, walls, and cells, which are generally linked with the extrusions and intrusions acting as crack precursors [42]). Consequently, the relatively less localized deformation in CoCrNi delays both fatigue crack initiation and propagation. Together, this finding extends our previous conclusion that CoCrNi shows superior LCF resistance than CoCrFeMnNi at RT [16] and 550 °C. Notably, the delayed crack propagation in CoCrNi is in line with its superior fatigue crack growth threshold compared to CoCrFeMnNi [43, 44], despite their similar fracture surface morphology (see Fig. A2 and associated text).

Notably, the Cr-rich precipitates have also been reported in CoCrFeMnNi after LCF loading at 550 °C [14] and long-term annealing at 500−700 °C [45-47]. The Cr-rich phases in CoCrFeMnNi were identified as the topologically close-packed σ phase and $M_{23}C_6$ carbides (with carbon contamination originating from the material processing steps) [46]. In this work, $M_{23}C_6$ carbides were also identified along grain boundaries of CoCrNi after high-temperature LCF loading for about ~10 h, with carbon contamination originating from the material processing steps. This finding suggests that the single-phase CoCrNi can decompose in the presence of carbon during high-temperature cycling loading. Together with the reports that no carbides were observed upon ex-situ annealing (for 200 h at 500 °C, without LCF loading) [48] or cycling at RT [16], it is suggested that the carbides precipitation requires both elevated temperature and applied stress/strain conditions. Furthermore, since Cr is known to be a strong σ phase stabilizer [45, 47] and that the σ phase was reported to precipitate in CoCrNi after creeping at 700 °C for more than 300 h [13], we conclude that σ-phase precipitation, if

any, is too slow at 550 °C to play a role during LCF loading. Besides, after 200 h at 500 °C during ex-situ annealing (without LCF loading), no σ phase was detected [48]. At this stage, it is therefore unclear whether σ-phase precipitation is too slow at 550 °C or if applied stress or strain may facilitate its precipitation.

Although this study is limited to the LCF behavior of CoCrNi at a typical medium strain amplitude (0.5%), the currently reported deformation mechanisms are expected to apply at lower strain amplitudes (*e.g.*, 0.3%, where planar slip is most likely to dominate as well, owing to the low-stress levels [15]). While, at higher strain amplitudes (*e.g.*, 0.7%), cross slip may become more critical. Future studies on understanding the strain-life (*i.e.*, Manson-Coffin) relation of CoCrNi under a wide range of strain amplitudes are envisaged.

Since the separation distance between Shockley partials mainly controls the deformation mechanisms in FCC alloys, the current findings obtained for CoCrNi are believed to be applicable for other FCC MPEAs (and conventional steels) with a low-SFE and a high shear modulus. Lastly, though a direct comparison of the fatigue properties between CoCrNi and conventional steels is beyond the scope of this work, the CoCrNi is anticipated to show higher fatigue resistance due to its higher strength and excellent ductility. Besides, massive carbide precipitation may be expected in austenitic stainless steels owing to their much more significant carbon concentration, which may affect the LCF behavior.

In summary, this work revealed the cyclic deformation behavior and underlying deformation mechanisms of the CoCrNi MPEA at 550 °C under a medium strain amplitude (0.5%). Compared to previous results reported for the CoCrFeMnNi alloy, CoCrNi exhibits higher cyclic strength, longer fatigue life, and continuous serrated flow. TEM investigations at different cyclic stages highlighted that the primary deformation mechanism corresponds to planar slip of dislocations dissociated into Shockley partials despite being at elevated temperatures. This may be related to the low SFE of CoCrNi, even at 550 °C, and eventually to a Suzuki effect, which likely leads to the occurrence of serrated flow by pinning/unpinning of dislocations. In contrast to the coexisting planar

and cross slip in CoCrFeMnNi, the prevalent planar slip in CoCrNi contributes to its longer fatigue life at 550 °C. Finally, the precipitation of ~0.3 Vol.% $M_{23}C_6$ carbides was observed along the grain boundaries, but we believe that its precipitation does not affect the LCF lifetime significantly.

This work can serve as a reference for understanding fatigue deformation mechanisms of FCC MPEAs (especially those with low SFEs) and also for guiding the design of more complex CoCrNi-based MPEAs with enhanced failure resistance.

Acknowledgments

Appendix
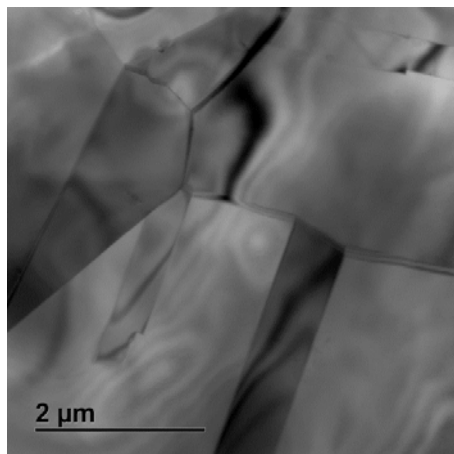
Fig. A1. A typical BF-TEM micrograph of CoCrNi in the recrystallized state shows low initial dislocation density.
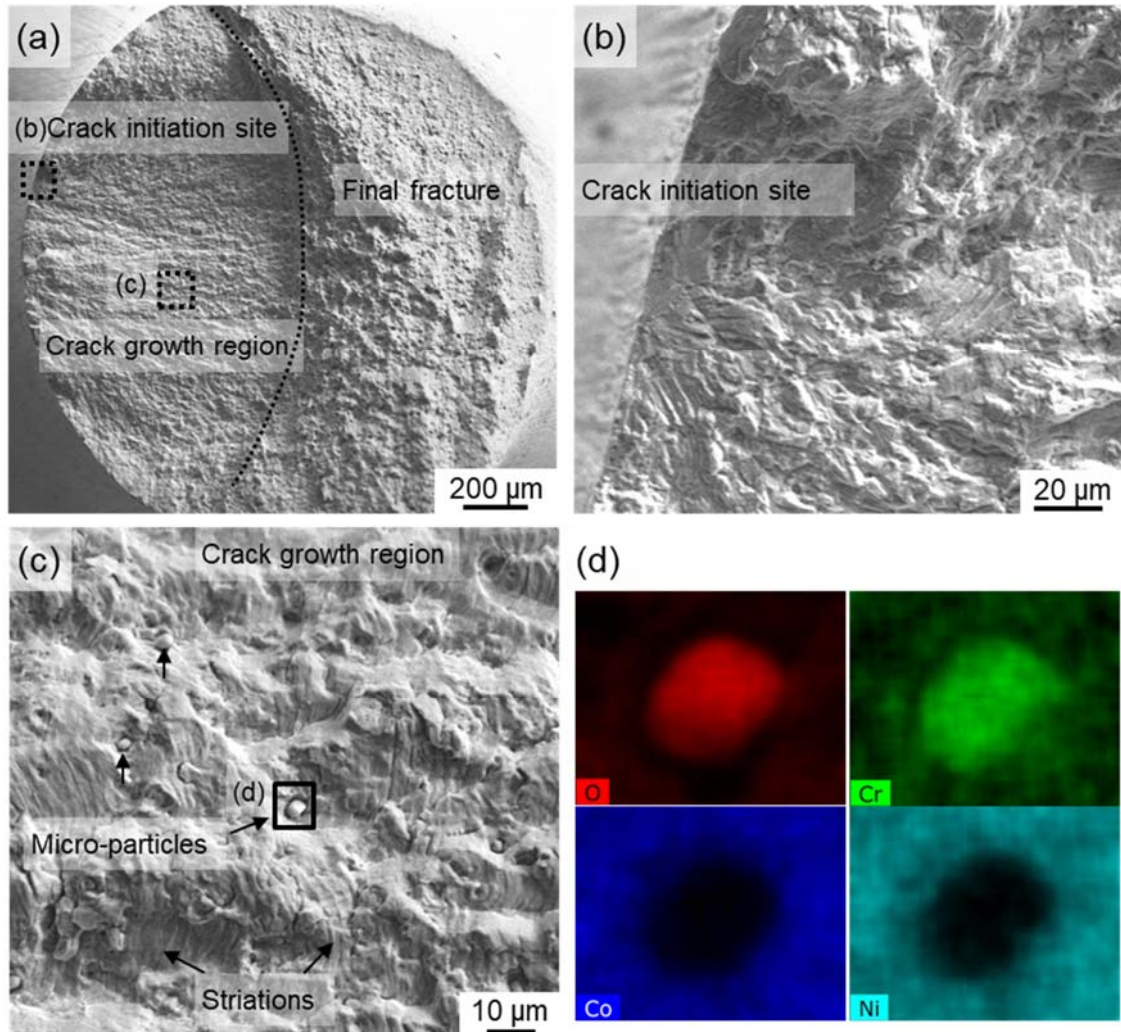
Fig. A2 Fracture surface of CoCrNi observed by SEM after LCF-testing at 550 °C under a strain amplitude of 0.5%: (a) overview of the whole specimen, enlarged view of (b) crack initiation site and (c) crack growth region, as well as (d) EDX elemental maps showing that the microparticles in (c) are Cr-rich oxides.

(Discussion on Fig. A2): The fracture surface morphology revealed crack initiation from the sample surface (see Fig. A2a-b), where slip bands introduced intrusions/extrusions and are believed to be the main crack initiation site. The crack growth region manifested striations (see Fig. A2c) due to crack-tip blunting and resharpening [49], indicating primarily transgranular crack growth mode. Besides, the micro-sized particles were also observed (see Fig. A2c), and EDS analyses revealed them to be Cr-enriched oxides (see

13

Fig. A2d). These microparticles were reported to originate from melting and casting [4]. It should be noted that these oxides (primarily those close to the sample surface) could act as crack initiation sites and accelerate crack propagation, thereby reducing the LCF life.
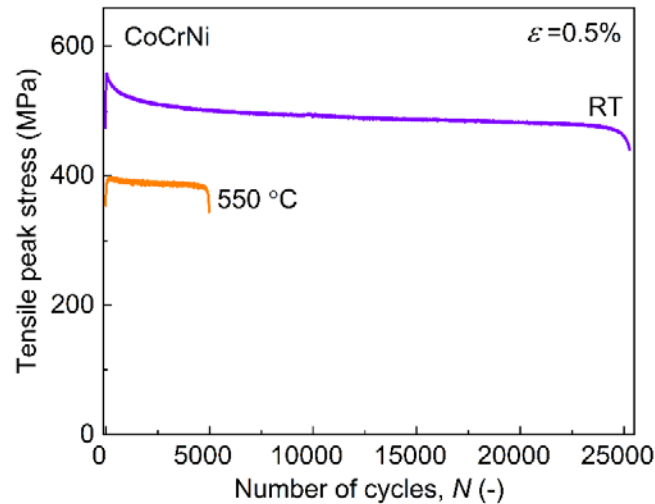
Fig. A3. Effect of temperature on cyclic stress responses of CoCrNi under a strain amplitude of 0.5%.

References

[1] B. Gludovatz, A. Hohenwarter, D. Catoor, E.H. Chang, E.P. George, R.O. Ritchie, Science 345 (6201) (2014) 1153-1158.

[2] B. Gludovatz, A. Hohenwarter, K.V. Thurston, H. Bei, Z. Wu, E.P. George, R.O. Ritchie, Nat Commun 7 (2016) 10602.

[3] G. Laplanche, A. Kostka, O. Horst, G. Eggeler, E.P. George, Acta Materialia 118 (2016) 152-163.

[4] G. Laplanche, A. Kostka, C. Reinhart, J. Hunfeld, G. Eggeler, E.P. George, Acta Materialia 128 (2017) 292-303.

[5] D. Hua, Q. Xia, W. Wang, Q. Zhou, S. Li, D. Qian, J. Shi, H. Wang, International Journal of Plasticity 142 (2021).

[6] C. Stephan-Scherb, W. Schulz, M. Schneider, S. Karafiludis, G. Laplanche, Oxidation of Metals 95(1) (2021) 105-133.

[7] M. Zhang, E.P. George, J.C. Gibeling, Acta Materialia 218 (2021).

[8] F. Otto, A. Dlouhý, C. Somsen, H. Bei, G. Eggeler, E.P. George, Acta Materialia 61(15) (2013) 5743-5755.

[9] M. Kawamura, M. Asakura, N.L. Okamoto, K. Kishida, H. Inui, E.P. George, Acta Materialia 203 (2021).

[10] L. Li, Z. Chen, S. Kuroiwa, M. Ito, K. Kishida, H. Inui, E.P. George, International Journal of Plasticity (2021).

[11] D. Xie, R. Feng, P.K. Liaw, H. Bei, Y. Gao, Scripta Materialia 212 (2022).

[12] M. Zhang, E.P. George, J.C. Gibeling, Scripta Materialia 194 (2021).

[13] D. Xie, R. Feng, P.K. Liaw, H. Bei, Y. Gao, Intermetallics 121 (2020).

[14] K. Lu, A. Chauhan, D. Litvinov, M. Walter, A.S. Tirunilai, J. Freudenberger, A. Kauffmann, M. Heilmaier, J. Aktaa, Materials Science and Engineering: A 791 (2020) 139781.

[15] K. Lu, A. Chauhan, D. Litvinov, J. Aktaa, International Journal of Fatigue 160 (2022).

[16] K. Lu, A. Chauhan, M. Walter, A.S. Tirunilai, M. Schneider, G. Laplanche, J. Freudenberger, A. Kauffmann, M. Heilmaier, J. Aktaa, Scripta Materialia 194 (2021) 113667.

[17] K. Lu, A. Chauhan, A.S. Tirunilai, J. Freudenberger, A. Kauffmann, M. Heilmaier, J. Aktaa, Acta Materialia 215 (2021) 117089.

[18] M. Heczko, V. Mazánová, C.E. Slone, M. Shih, E.P. George, M. Ghazisaeidi, J. Polák, M.J. Mills, Scripta Materialia 202 (2021).

[19] S. Picak, T. Wegener, S.V. Sajadifar, C. Sobrero, J. Richter, H. Kim, T. Niendorf, I. Karaman, Acta Materialia 205 (2020).

[20] S.A.A. Shams, G. Jang, J.W. Won, J.W. Bae, H. Jin, H.S. Kim, C.S. Lee, Materials Science and Engineering: A 792 (2020) 139661.

[21] M.-Y. Luo, T.-N. Lam, P.-T. Wang, N.-T. Tsou, Y.-J. Chang, R. Feng, T. Kawasaki, S. Harjo, P.K. Liaw, A.-C. Yeh, S.Y. Lee, J. Jain, E.W. Huang, Scripta Materialia 210 (2022).

[22] A. Chauhan, D. Litvinov, J. Aktaa, International Journal of Fatigue 93 (2016) 1-17.

[23] B. Li, Y. Zheng, J. Zhao, S. Shi, Z. Zhang, X. Chen, Materials Science and Engineering: A 818 (2021).

[24] A. Chauhan, J. Hoffmann, D. Litvinov, J. Aktaa, Materials Science and Engineering: A 707 (2017) 207-220.

[25] N.L. Okamoto, S. Fujimoto, Y. Kambara, M. Kawamura, Z.M. Chen, H. Matsunoshita, K. Tanaka, H. Inui, E.P. George, Scientific Reports 6 (2016) 35863.

[26] C. Wagner, A. Ferrari, J. Schreuer, J.-P. Couzinié, Y. Ikeda, F. Körmann, G. Eggeler, E.P. George, G. Laplanche, Acta Materialia 227 (2022).

[27] L. Rémy, A. Pineau, B. Thomas, Materials Science and Engineering 36(1) (1978) 47-63.

[28] S. Huang, W. Li, S. Lu, F. Tian, J. Shen, E. Holmström, L. Vitos, Scripta Materialia 108 (2015) 44-47.

[29] D. Caillard, J.-L. Martin, Thermally activated mechanisms in crystal plasticity, Elsevier2003.

[30] W. Cai, V.V. Bulatov, J. Chang, J. Li, S. Yip, in: F.R.N. Nabarro, J.P. Hirth (Eds.), Dislocations in Solids, Elsevier2004, pp. 1-80.

[31] M. Schneider, E.P. George, T.J. Manescau, T. Záležák, J. Hunfeld, A. Dlouhý, G. Eggeler, G. Laplanche, International Journal of Plasticity 124 (2020) 155-169.

[32] R. Sandhya, K.B.S. Rao, S. Mannan, R. Devanathan, International journal of fatigue 23(9) (2001) 789-797.

[33] M. Gerland, R. Alain, B. Ait Saadi, J. Mendez, Materials Science and Engineering: A 229(1) (1997) 68-86.

[34] K. Lu, A. Chauhan, F. Knöpfle, J. Aktaa, Materials Research Letters 10(6) (2022) 369-376.

[35] X. Feaugas, Acta Materialia 47(13) (1999) 3617-3632.

[36] P. G. McCormick, Acta Metallurgica 20(3) (1972) 351-354.

[37] S. Hong, K. Lee, S. Lee, International Journal of Fatigue 27(10-12) (2005) 1420-1424.

[38] V.S. Srinivasan, M. Valsan, R. Sandhya, K. Bhanu Sankara Rao, S.L. Mannan, D.H. Sastry, International Journal of Fatigue 21(1) (1999) 11-21.

[39] Z. Wu, H. Bei, G.M. Pharr, E.P. George, Acta Materialia 81 (2014) 428-441.

[40] A. Durand, L. Peng, G. Laplanche, J.R. Morris, E.P. George, G. Eggeler, Intermetallics 122 (2020) 106789.

[41] H. Mughrabi, Acta Materialia 61(4) (2013) 1197-1203.

[42] P. Lukáš, L. Kunz, Philosophical Magazine 84(3-5) (2004) 317-330.

[43] J. Rackwitz, Q. Yu, Y. Yang, G. Laplanche, E.P. George, A.M. Minor, R.O. Ritchie, Acta Materialia 200 (2020) 351-365.

[44] K.V.S. Thurston, B. Gludovatz, A. Hohenwarter, G. Laplanche, E.P. George, R.O. Ritchie, Intermetallics 88 (2017) 65-72.

[45] F. Otto, A. Dlouhý, K.G. Pradeep, M. Kuběnová, D. Raabe, G. Eggeler, E.P. George, Acta Materialia 112 (2016) 40-52.

[46] E.J. Pickering, R. Muñoz-Moreno, H.J. Stone, N.G. Jones, Scripta Materialia 113 (2016) 106-109.

[47] G. Laplanche, Acta Materialia 199 (2020) 193-208.

[48] B. Schuh, B. Volker, J. Todt, K.S. Kormout, N. Schell, A. Hohenwarter, Materials (Basel) 11(5) (2018) 662.

[49] S. Suresh, Fatigue of materials, Cambridge university press1998.